ChemSusChem

Research Article
doi.org/10.1002/cssc.202300482

Chemistry Europe
European Chemical Societies Publishing

www.chemsuschem.org

Density Functional Theory-Based Protocol to Calculate the Redox Potentials of First-row Transition Metal Complexes for Aqueous Redox Targeting Flow Batteries

Noura Rahbani,[a] Piotr de Silva,*[b] and Emmanuel Baudrin*[a]

Transition metal complexes are a promising class of redox mediators for targeting redox flow batteries due to the tunability of their electrochemical potentials. However, reliable time-efficient tools for the prediction of their reduction potentials are needed. In this work, we establish a suitable density functional theory protocol for their prediction using an initial experimental data set of aqueous iron complexes with bidentate ligands. The approach is then cross-validated using different complexes found in the redox-flow literature. We find that the solvation model affects the prediction accuracy more than the functional or basis set. The smallest errors are obtained using the COSMO-RS solvation model (mean average error (MAE) = 0.24 V). With implicit solvation models, a general deviation from experimental results is observed. For a set of similar ligands, they can be corrected using simple linear regression (MAE = 0.051 V for the initial set of iron complexes).

Introduction

As the use of renewable energy sources increases, the integration of safe, reliable, and affordable large-scale electrochemical storage devices into the grid is needed to increase its stability and reliability.[1] For this purpose, redox flow batteries (RFBs) are a promising technology. In an all-liquid RFB, the active species are dissolved in electrolytes and stored in external tanks. During operation, external pumps continuously flow the electrolytes through the tanks and the cell stack(s) where electrochemical conversion takes place. This modular design lends RFBs their unique capability to decouple power and energy and leads to their inherent scalability. A main issue for all-liquid RFBs however is their low energy densities (~ 50 Wh L^{-1} for the vanadium redox flow battery).[2] For scaling up the energy, an electrolyte couple with higher energy density (higher concentration or cell potential) or a larger quantity of electrolyte is needed. In aqueous RFBs, the cell potential range is limited to that of the electrochemical stability of water. Subsequently, the route to increasing their energy density is linked to the concentration of the electroactive species.

Alternatively, new RFB architectures have been proposed, like the redox targeting-based redox flow battery (RT-RFB) first introduced in 2013 by the group of Wang,[3] which incorporates electroactive solid "booster" materials in the system. During operation, this added material is kept in the tanks while dissolved redox mediator species circulate through the cell stack. The first proposed systems required two redox mediators per electrolyte, having redox potentials sandwiching that of the solid. In most cases, the inherent difference in the charge and discharge potentials of the battery leads to a high voltage inefficiency. However, a recent report showed that kinetic factors also play an important role, and dual mediator systems with good kinetics could present high voltage efficiency.[4] This inefficiency issue could also be averted by using single molecule redox targeting (SMRT),[5] for which in each half-cell there is only one mediator whose potential matches that of the insertion material. This works as the potential of the redox mediator follows Nernst's relationship. Indeed, during charging of a posolyte, the initially reduced form of the mediator is pumped through the cell and oxidized. The posolyte redox potential would then increase and become higher than the potential of the solid allowing electron transfer to take place. The charge will proceed under flow of the mediator (oxidized in the cell/reduced in the tank) up to the complete oxidation of the solid. During discharge the opposite processes would occur. In RT-RFB, the energy density of the cell is no longer limited by the amount of dissolved redox species but depends mostly on the quantity of solid insertion material placed in the tank and the extent of its utilization.

Since the introduction of RT-RFBs, reported SMRT systems usually have been using iron cyanide, metallocene derivatives, or organic compounds as posolyte mediators and organic compounds as negolite mediators.[5–10] A targeting vanadium redox flow battery has also been proposed.[11] In their study on the thermodynamics of RT-RFBs, Moghaddam et al. demonstrated the importance of carefully choosing redox mediators

[a] N. Rahbani, Prof. E. Baudrin
Laboratoire de Réactivité et Chimie des Solides, CNRS UMR7314
Université de Picardie Jules Verne
33 Rue St-Leu, 80039 Amiens, Cedex (France)
E-mail: emmanuel.baudrin@u-picardie.fr
[b] Prof. P. de Silva
Department of Energy Conversion and Storage
Technical University of Denmark
Anker Engelunds Vej 301, 2800 Kongens Lyngby, Copenhagen (Denmark)
E-mail: pdes@dtu.dk

Supporting information for this article is available on the WWW under https://doi.org/10.1002/cssc.202300482

and solid boosters with matching redox potentials.[12] Comparing the calculated state of charge (SoC) curve of a hypothetical ideal redox mediator with the experimental SoC curve of a copper hexacyanoferrate solid booster, they showed that in a battery operating between 5 and 95% SoC of the mediator, the maximum accessible capacity of the solid booster is 80% of the theoretical one. However, when the potential of the mediator is shifted by 50 mV in either direction, this drops to 50% of utilization.

As such, we feel that metal-organic complexes are promising redox mediators due to the flexibility of their redox potentials and the possibility to control them through the choice of the metal center and the ligand(s). It is well established that ligand coordination changes the redox potential of transition metal systems and increases the solubility of metals at various pHs.[13] As a first step, we choose to focus on iron complexes as potential negolyte mediators, as iron is abundant, cheap, and non-toxic. Iron complexes offer a wide range of potentials (from +1.20 V to −1.14 V) as reported by Esswein et al.[14] and Gao et al.[15] Ligands with harder donor sites are expected to interact with/complex iron(III) more than iron(II) leading to a decrease in the reduction potential of the formed iron species compared to the aquo complex.

Given the arena of ligands and their molecular engineering possibilities, this offers a vast chemical space to explore, for which we could take advantage of quantum chemical simulations.[16] Density functional theory (DFT) calculations have already been used for the high throughput screening of organic molecules for RFBs with accuracies in the vicinity of 70 mV for the calculated redox potentials.[17–20] However, calculations on metallo-organic complexes usually result in larger differences between experimental and calculated redox potentials (up to 1 V or more) and have consequently been used for studying trends of the ligand effect rather than for accurate predictions.[13,21] Recently, a machine learning protocol was proposed for high throughput screening of transition metal complexes for various applications.[22] In the proposed workflow, DFT calculations were performed on a select set of complexes to improve the performance of the model, as a reliable method for predicting properties is needed in any computational workflow. For this purpose, DFT still offers a good trade-off between computational cost and accuracy. The main goal of the present work is to establish a DFT calculation protocol for the quick and reliable prediction of redox potentials of octahedral transition metal complexes to be used for the screening of redox mediators for aqueous TRFBs. To do this, high spin iron complexes forming 5-membered chelate rings with bidentate ligands have been synthesized and their redox potential computed to establish the best calculation protocol. This is then extended and generalized to titanium(IV) and low spin iron(II) complexes found in the redox-flow literature.

Results and Discussion

DFT protocol for calculating redox potentials

The redox potentials (Figure 1a) of five iron complexes with bidentate ligands having oxygen donor sites were initially used to establish the computational protocol. The experimental redox potentials of free iron (aqua complex), iron maltol, iron catechol, iron kojate and iron deferiprone (Figure 2) were obtained by synthesis via a simple mixing procedure followed by cyclic voltammetry, and that of iron salicylate was obtained from the literature.[14] As the ligands have oxygen donor sites, they are expected to stabilize iron(III) and push the redox potentials to negative values. Even with this limited set of ligands, the redox potential of the iron couple varies over a wide range from −0.23 V to −0.83 V, as detailed in Figure 1. Cyclic voltammograms (CVs) of the synthesized complexes collected at the required pH for the formation of hexacoordinated iron (ML_3 complex) show quasi-reversible behavior (Figure S2 in the Supporting Information), with peak separation ranging from 88 mV for iron maltol and iron deferiprone and 431 mV for iron catechol.

The required pHs were identified by tracking the evolution of the complexes with pH using UV/Vis spectroscopy and cyclic voltammetry. Figure 1b and c show the case of the iron maltol complex. We could deduce from the UV/Vis spectra that at a pH of 3 the complex formed of iron with two ligands (ML_2) is already present, with a maximum absorption at a wavelength of $\lambda_{max}=505$ nmand the full complex (ML_3) is formed at pH 5 and above with $\lambda_{max}=472$, 410 nm. At higher pH values the absorbance begins to drop as a precipitate forms in the solution. Similar conclusions could be drawn from the cyclic voltammograms. The potential at pH 3 is +0.4 V, which is close to that of free iron. At pH 5 the potential is shifted to −0.23 V. This potential remains stable at higher pH values indicating that the ML3 complex has already formed. The current density at pH 7 is lower than at pH 5 as a precipitate forms in the solution.

The redox potentials of the complexes were then calculated using the ADF[23] software. Geometry optimizations were first performed in both vacuum and solvated phase using the COSMO[24] solvation model to compare the direct and indirect solvation methods. However, the geometries proved difficult to converge in the solvated phase, with imaginary frequencies remaining even after successive attempts with strict convergence criteria. Keeping to the goal of establishing a fast protocol for screening, the rest of the calculations were performed using the indirect method: solvated state total energies were obtained by performing single point calculations on geometries optimized in the gas phase. This also allowed the use of the SM12[25] solvation model which could not be used for geometry optimizations.

The redox potentials of the iron complexes were calculated at the B3LYP/TZP[26] level using the COSMO,[24] SM12,[25] and COSMO-RS[27,28] solvation models. Scatter plots of computed vs. experimental redox potentials are presented in Figure 3, with the mean absolute error (MAE) and the coefficient of determination (R^2) reported in the legends. The reported values

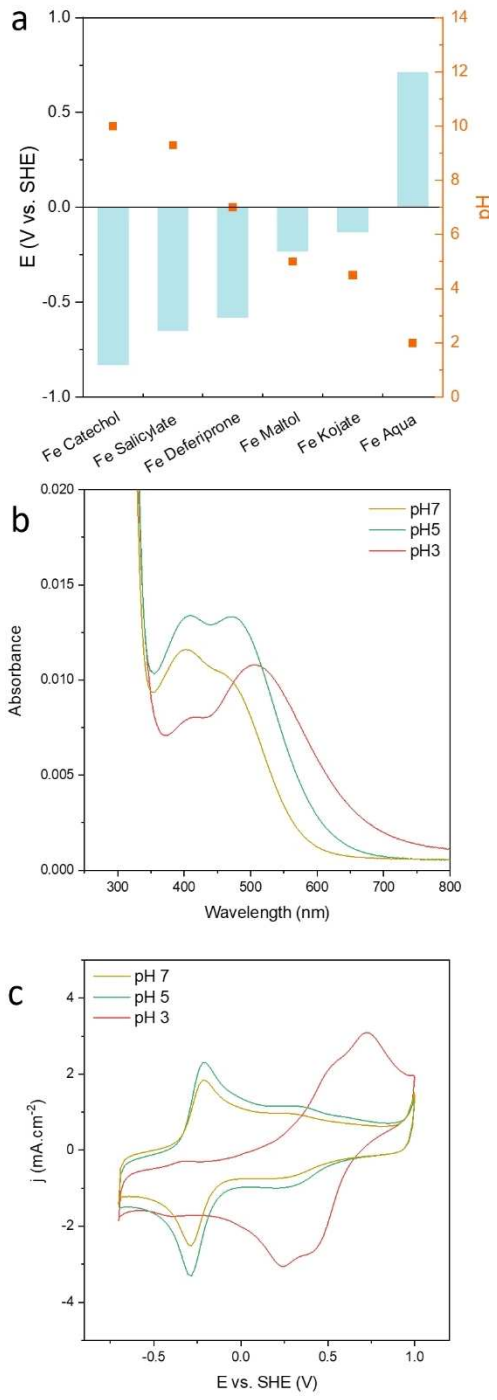

Figure 1. (a) Experimental redox potentials (blue, bars) of the ML_3 complexes and the pHs at which they form (orange, square markers). (b, c) Example of the experimental determination of pH and redox potential of the ML_3 complexes, here iron maltol. (b) UV/Vis spectra collected of the 10 mM iron maltol solutions 1:3 metal to ligand ratio in 0.5 M Na_2S0_4 using a 1 mm path length cuvette. (c) Cyclic voltammograms of the same solutions performed at a scan rate of 200 $mV\,s^{-1}$ using an Ag/AgCl reference electrode; reported here vs. the standard hydrogen electrode.

correspond to the high-spin state, which was the predicted ground state for all the complexes. While hybrid functionals are thought to favor high spin states, in a study on iron(II), iron(III), and iron(IV) complexes Verma et. al found that hybrid functionals including B3LYP predicted 13 out of 14 ground spin states correctly.[29]

All the methods show high average errors on the calculated redox potentials, between 0.3 V and 0.8 V. Of the implicit solvation methods, SM12 performs better than COSMO, but the lowest errors are obtained using COSMO-RS, which combines quantum chemistry with statistical mechanics. The COSMO-RS model in ADF is optimized to be used at the BP86/TZP level,[30] with a small core approximation and the inclusion of scalar relativistic effects using the ZORA[31] formalism. Here, the redox potentials were calculated from solvation free energies obtained in COSMO-RS using these standard settings and the gas-phase energies and free energy corrections obtained from the B3LYP/TZP calculations.

For the three solvation models, the deviation from experimental results increases with increasing overall charge of the complex, with the biggest errors for iron catechol and iron salicylate, both holding high negative charge of −3 for the iron(III) complex, and free iron. The errors on the highly charged species are most likely due to shortcomings of the implicit solvation models; it was previously shown that using explicit solvation including two solvation shells could improve the prediction of the redox potential of the iron aqua complex and other transition metal aqua complexes[32] as well as the redox potentials of quinones,[33] but these methods are time intensive for the user and computationally expensive, which makes them impractical for application in screening. However, the values calculated using the implicit solvation models have a good R^2, which allows for a simple correction via linear regression. Figure 3b offers a comparison between the initially calculated potentials and the new predicted ones using SM12. When corrected, the new MAEs on COSMO and SM12 calculations become comparable and in the vicinity of 0.1 V. This is apparent in the scatter plots, as the corrected redox potentials (in black markers) lie close to the identity line ($y=x$).

In an attempt to improve accuracy without compromising time efficiency, the potentials were calculated using large basis sets on iron and smaller ones for the organic ligands (Figure 4). The triple-zeta with two polarization functions (TZ2P) and core triple-zeta/valence quadruple-zeta with four sets of polarization functions (ZORA/QZ4P) basis sets were used for iron, with the smaller double-zeta polarized (DZP) or triple-zeta polarized (TZP) basis set for the rest of the atoms. ZORA/QZ4P is the largest basis set provided within the ADF basis function library. Only the SM12 solvation model was used, since the TZP basis set is recommended by ADF for the COSMO-RS model.[30] The performances of the basis sets are comparable, with differences in MAE in the range of 0.1 V. The calculations using the TZP basis set for all elements (MAE = 0.49 V) show smaller error than those using mixed sets, except for the ZORA/QZ4P-DZP combination (MAE = 0.46 V). However, the difference in MAE is not significant enough to warrant using the bigger basis set. Correcting the values using linear regression leads to a 10-fold reduction in the mean average errors to 0.06–0.08 V (Figure 4b). Calculations using the augmented triple-zeta polarized

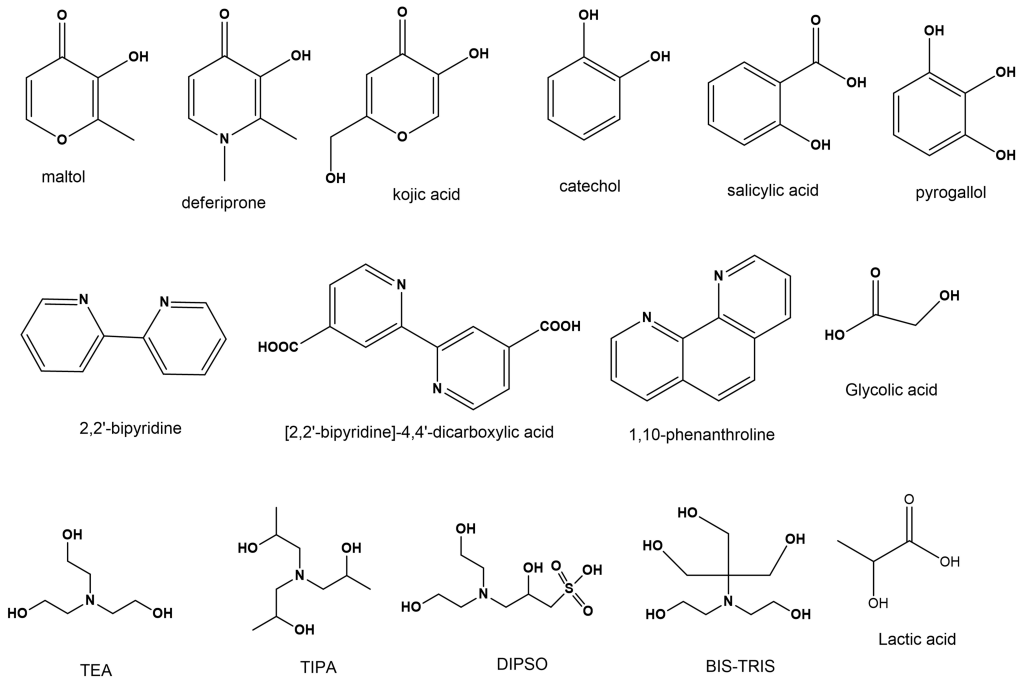

Figure 2. Chemical structures of the different ligands examined in this study.

(AUG-TZP) basis set were also attempted but lead to convergence issues.

After the effect of basis set size was studied, we moved our attention to the electronic structure method. Initially, the B3LYP functional was chosen due to its popularity with both organic and non-organic molecules, and its use in other studies on calculating redox potentials of transition metal complexes.[22,33] However, some benchmarking studies show that its popularity is not always well justified.[34,35] While the relationship between accuracy and functional choice is well acknowledged, the most suitable methods change with the type of system under study. As such, there are no fixed rules for choosing a functional, and evaluating them individually will be a tedious task. For this, we decided to benefit from the post-SCF energy functional feature in ADF, which provides reasonable estimates for total energies from different XC functionals from one calculation at negligible added cost. To do this, one functional (here, B3LYP) is chosen for the potential, and determines the self-consistent charge density, and the rest are successively used for the energy expression that is used to evaluate the XC part of the total energy.

The post-SCF calculations were performed with the single point calculation in both COSMO and SM12. As this feature could not be applied for calculating the free energy correction, those from the previous B3LYP calculations were used to draw general conclusions from the results (Table S1). First, it is still clear that the SM12 solvation model outperforms COSMO; the MAE across all functionals and all complexes is 0.85 V for SM12 but 1.17 V for COSMO. Second, it could be concluded that for the complexes, hybrid functionals outperform GGAs with the lowest performing 10% always being GGAs, and the top performing 10% being hybrids. However, for the iron-aqua complex the opposite holds true. This disagreement between the trends for "free" and complexed iron holds for most observations. When only taking hybrid functionals into account, M05 and M06 are the two lowest performing functionals for the complexes (25% HF exchange, MAE = 1.02 V, SM12) while the best performing are M05-2X and M06-2X (56% HF exchange, MAE = 0.24 V, SM12). The opposite holds true for free iron where M05-2X and mPW1K have the largest errors (MAE = 1.08 V, SM12), while M05 and M06 have the smallest errors (0.39 V, SM12). The B3LYP, B3LYP* and D-B3LYP functionals, are comparable, with an average difference of 0.10 V between the extremities. For the complexes, B3LYP performs best, and B3LYP* has the largest error; for free iron, again, the reverse is observed with B3LYP* outperforming D-B3LYP and B3LYP. The redox potentials of the complexes were then calculated using the M06-2X functional for both the potential and the energy expression. This led to a reduction in the MAE from 0.55 to 0.46 V using the TZP basis set and SM12.

Gaussian vs. Slater type orbitals

A drawback of using hybrid functionals in ADF is that analytical frequency calculations are not supported. As a result, time consuming numerical frequency calculations need to be used. As such, switching to a software that allows for analytical frequency calculations could save time, and the redox potentials were re-calculated using the Gaussian 16[36] software and the SMD solvation model, which is their recommended solvation model for thermodynamic properties. The computa-

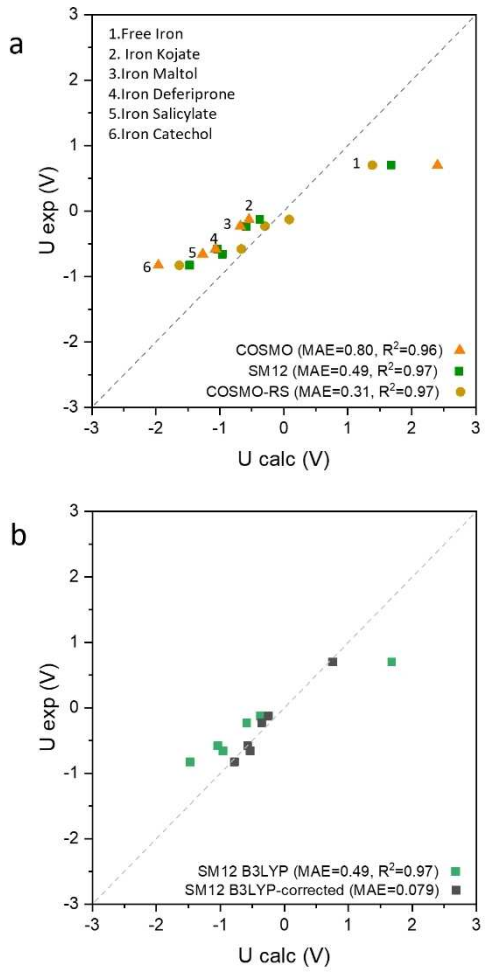

Figure 3. Experimental-computational correlation plots comparing different

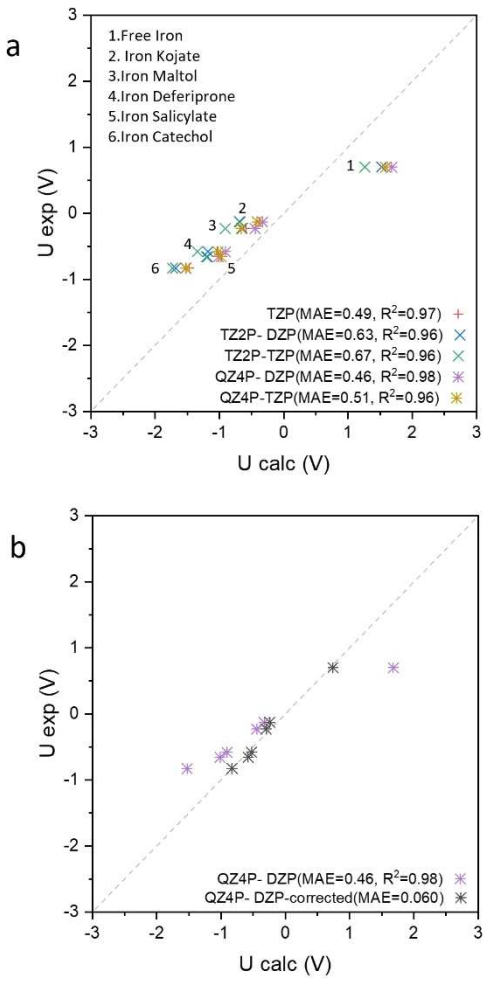

Figure 4. Experimental-computational correlation plots comparing calculations using mixed basis sets with the SM12 solvation model and the B3LYP functional: TZP for all elements (red, cross), TZ2P for iron and DZP (blue, x) or TZP (green, x) for smaller elements, ZORA/QZ4P for iron and DZP (purple, star) or TZP (golden, star) for smaller elements. (a) Overlay of the values obtained with the 5 different basis sets. (d) Comparison between calculated (colorful markers) and corrected (black markers) redox potentials for the ZORA/QZ4P-DZP basis set which showed the lowest MAE. The dashed line represents $y = x$.

tional times were significantly reduced from 2–4 days down to hours when using 40 CPU cores. This shift also allows the comparison of molecular orbital representations: ADF uses Slater-type orbitals (STOs) while Gaussian uses Gaussian-type orbitals (GTOs). STOs are closest to the mathematical expressions derived from solving the problem of the hydrogen atom, while with GTOs the form of the radial decay is changed, so the orbital-like functions have the form of a gaussian function. As a result, GTOs are computationally cheaper but expected to be less accurate.

Since the use of analytical frequency calculations significantly cuts down on time, larger basis sets could be used for all the atoms in the complexes. The redox potentials were calculated using the B3LYP and then the M06-2X functionals, and the 6-31 + G(d),[37] 6-311 + G(d),[38] cc-pVTZ[39] basis sets. The basis sets were compared by using either the same basis set for all the calculations, or mixtures where the smaller 6-31 + G(d) or 6-311 + G(d) sets are used for the expensive geometry and frequency calculations and cc-pVTZ is only used for solvation single point calculations. Like in ADF, the geometry optimizations performed with the augmented basis set aug-cc-pVTZ proved difficult to converge.

The mean errors using the B3LYP functional ranged from 0.61 to 0.71 V and were lower for calculations using only one basis set, as also observed by Konezny et. al.[40] The performance of the 6-31 + G(d), 6-311 + G(d), cc-pVTZ basis sets is comparable, and when corrected via linear regression the predicted redox potentials align with the experimental potentials, with MAEs in the vicinity of 0.07 V. The 6-311 + G(d) basis set performs similarly to the TZP in ADF, with a mean average error of 0.56 V before correction, and 0.078 V after. Lower errors were achieved using the M06-2X functional, with the average error across all basis sets 0.15 V lower than that using B3LYP (Table 1, Figure 5a,b). As with B3LYP, fluctuation between basis sets using the same functional are less notable. Calculations performed at the M06-2X/6-311 + G(d) level have the lowest average error of 0.37 V, comparable to that using COSMO-RS (MAE = 0.31 V), and 0.2 V lower that that with B3LYP.

Table 1. Mean average errors on the redox potentials calculated using B3LYP and M06-2X with various basis sets and the SMD solvation model in Gaussian 16.

Method	MAE [V]	MAE-corr [V]
B3LYP/631+G(d)	0.64	0.066
B3LYP/6311+G(d)	0.56	0.067
B3LYP/cc-pVTZ	0.61	0.078
B3LYP/631+G(d), cc-pVTZ	0.71	0.067
B3LYP/6311+G(d), cc-pVTZ	0.69	0.063
M06-2X/631+G(d)	0.49	0.060
M06-2X/6311+G(d)	0.38	0.051
M06-2X/cc-pVTZ	0.52	0.064
M06-2X/631+G(d), cc-pVTZ	0.51	0.060
M06-2X/6311+G(d), cc-pVTZ	0.54	0.055

The geometries obtained from the calculations in Gaussian 16 were then used to calculate the COSMO-RS solvation energies of the complexes. As the geometries were re-optimized in BP86 for the calculations, the potentials obtained from G16/B3LYP and those from G16/M06-2X had the same MAE of 0.12 V, which is also the lowest MAE values obtained without linear regression corrections. As seen in Figure 5c, all the calculated values lie close to the identity except for iron catechol, which has a high charge (−3 for the iron(III) complex).

Application to different types of complexes

So far, we have identified two methods for the determination of the reduction potentials of our initial set of iron complexes. In the first method, energies in the solvated state are obtained using the SMD solvation model and are used to calculate the reduction potentials, after which a linear regression is used for corrections. In the second method, solvation energies are obtained using the COSMO-RS model are added to the gas phase energies and used to obtain the reduction potentials; no corrections are needed. For both, geometries are optimized in the gas phase at the B3LYP/6311+G(d) or M06-2X/6311+G(d) level. To assess the transferability of the protocols beyond our initial set of iron complexes different complexes whose experimental redox potentials are known in the literature are used.

First, titanium(IV/III) complexes from a patent by Lockheed Martin[41] which have similar coordination environments are used: titanium catechol, titanium salicylate, and titanium pyrogallol (Figure 2). The MAEs on the redox potentials obtained using the B3LYP functional (ADF/TZP/SM12 and G16/6-311+G(d)/SMD) are comparable to each other and to those of the iron complexes. In these cases, the trend of increasing error with decreasing redox potential continues, and the predictions could be significantly corrected using linear regression. The correction was implemented using the linear regression obtained using only the iron complexes as a cross-validation of the predictive power of the approach; the MEA of the full set decreases from 0.58 V to 0.12 V (Figure S4).

The M06-2X functional and the COSMO-RS model outperform B3LYP, with MAEs of 0.29 V and 0.16 V respectively. Here, applying the linear regression does not correct the values for the titanium complexes and leads to insignificant change in the MAE (Figure S4). Rather than follow a general trend, both

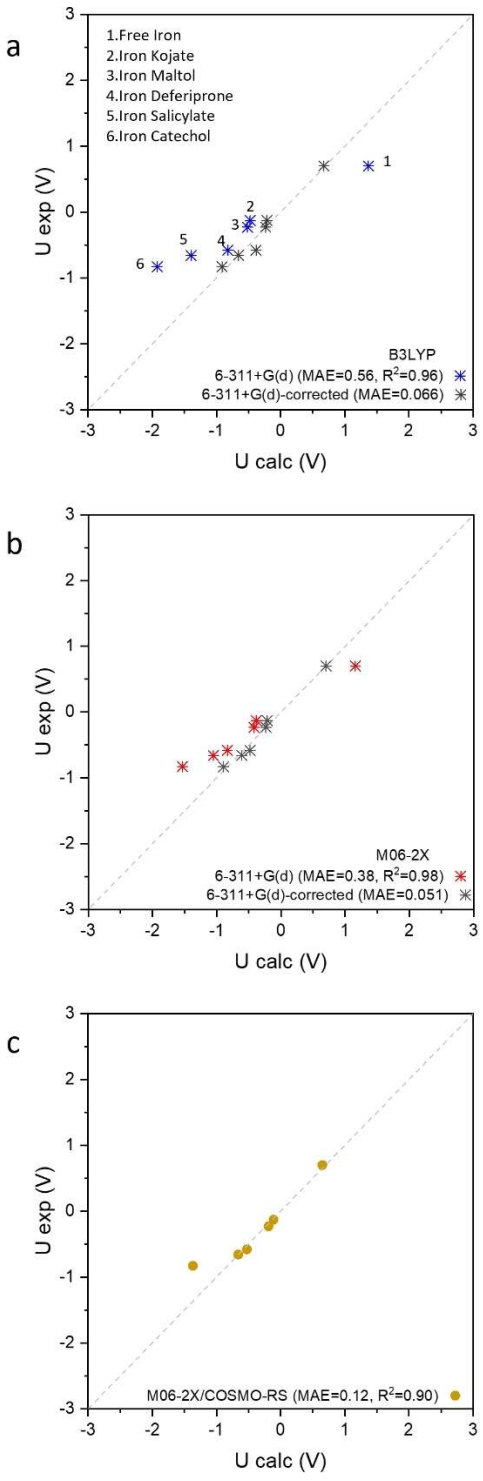

Figure 5. Experimental-computational correlation plots comparing the B3LYP (a) and M06-2X (b) functionals using the SMD solvation model and 6-311+G(d) basis set, and the COSMO-RS solvation model using the obtained geometries (c, d). The colored and black markers represent the calculated and corrected data, respectively. The dashed line represents $y=x$.

methods accurately predict redox potentials but with outliers which become quite apparent here: iron catechol, iron salicylate, and free iron. Higher errors are expected for highly charged molecules; however, the calculations are accurate for titanium complexes with the same charge as the iron complexes in question. The higher errors on iron complexes could then be due to a combination of high charges and the possibility of different spin states, which is not the case for titanium.

Next, the three methods were used to calculate the redox potentials of low spin octahedral iron(II) complexes with cyanide, bipyridine, phenanthroline and of heteroleptic iron(II) complexes of cyanide and 2,2′-bipyridine-4,4′-dicarboxylic acid, the experimental redox potential of which were gathered from the literature.[42,43] With both B3LYP/SMD and M06-2X/SMD, the low spin iron complexes lie on a different trendline than that of the high spin iron and titanium complexes (blue crosses, Figure 6a and b). The two trend lines share similar slopes (0.60 and 0.59 for B3LYP), hinting that the same systematic error could be affecting the low spin iron complexes more than the high spin ones. Once again, the errors are minimized when the COSMO-RS solvation model is used, with the MAE dropping from 0.58 V to 0.24 V for M06-2X, and the values for the different groups of complexes lie close to the identity line, Figure 6c, blue markers. The redox potential of the iron hexacyanide complex was also calculated but showed exceptional deviation from experimental value at −0.56 V (experimental value +0.37 V). This exception was also demonstrated by Liang et al.[44] and Hughes and Friesner,[45] whose calculated reduction potentials also showed high deviation from the experimental value (−0.34 V and −0.33 V respectively). This could be due to the high crystal field stabilization energy of the complex and its high negative charge. Liang et al. also noted that while adding diffuse functions helped reduce the error for this complex, other measures like using larger basis sets did not affect the $Fe(CN)_6$ complex as it did the others. As this complex is an exceptional outlier, it was not used in the comparison of the three methods.

The redox potentials of trigonal bipyramidal iron(III) complexes with triethanolamine derivatives (triethanolamine (TEA), trisopropanolamine (TIPA), 3-[bis (2-hydroxyethyl) amino]-2-hydroxypropanesulfonic acid (DIPSO), and BIS-TRIS, Figure 2), and of iron(III) complexes with straight chain acidic ligands (lactic acid and glycolic acid) found in the redox-flow literature were also calculated.[14,46–49] As with the rest, the accuracy increases going from B3LYP, to M06-2X and finally by using the COSMO-RS solvation model, but the errors remain higher for the trigonal bipyramidal complexes than for the other groups. The results obtained from the three methods for all the complexes are depicted in Figure 6, and the redox potentials predicted using M06-2X/SMD, M06-2X/SMD corrected, and M06-2X/COSMO-RS are compared in Table 2.

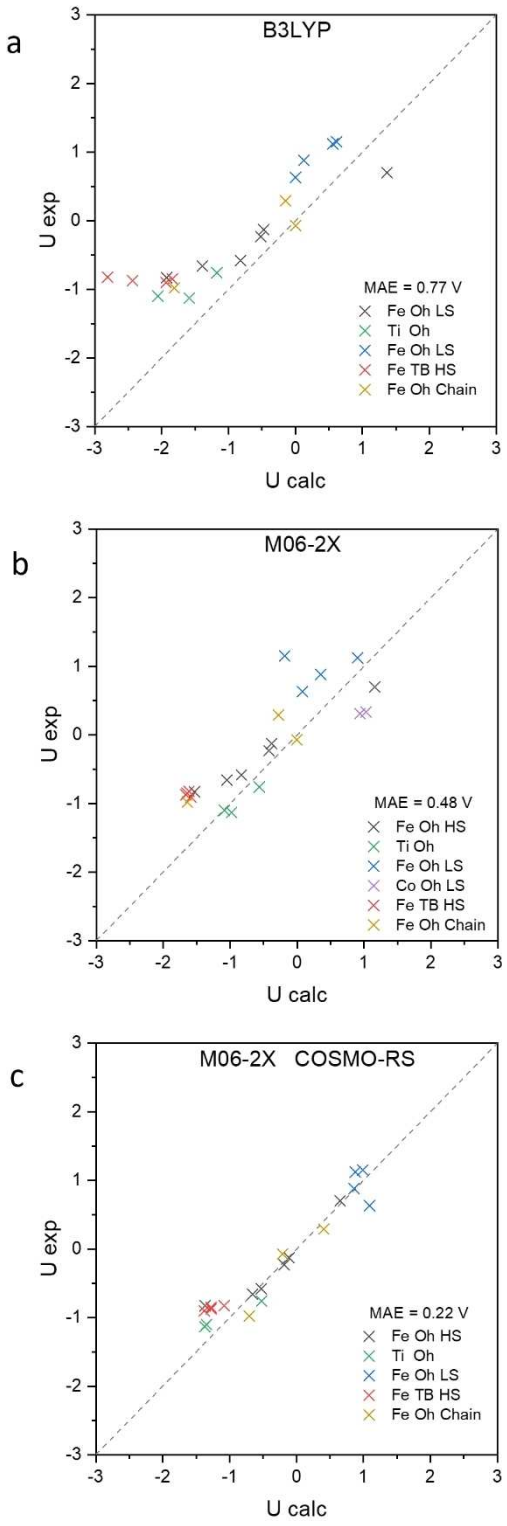

Figure 6. Experimental-computational correlation plots for all complexes obtained using the B3LYP (a) and M06-2X (b) functionals and SMD solvation model and using M06-2X geometries with the COSMO-RS solvation model (c). The groups are high spin octahedral iron complexes (black), octahedral titanium complexes (green), low spin octahedral iron complexes (blue), low spin octahedral cobalt complexes (purple), and high spin trigonal bipyramidal iron complexes (red). The dotted lines represent $y = x$.

Table 2. Calculated, corrected, and experimental redox potentials at the M06-2X/6-311+G(d) level of theory with SMD or COSMO-RS solvation models. Corrected potentials are obtained using the correlation curve of the initial set of iron complexes (Fe Aqua through Fe Catecholate). All are for the ML_3 complex unless stated otherwise.

Complex	Charge	$U_{M06\text{-}2X}$ [V]	U_{CORR} [V]	UCOSMO	U_{EXP} [V]
Fe Aqua	$2^+/3^+$	1.16	0.70	0.65	0.70
Fe Kojate	$1^-/0$	−0.38	−0.21	−0.11	−0.13
Fe Maltolate	$1^-/0$	−0.42	−0.23	−0.19	−0.23
Fe Deferiprone	$1^-/0$	−0.83	−0.48	−0.53	−0.58
Fe Salicylate[41]	$4^-/3^-$	−1.05	−0.61	−0.66	−0.66
Fe Catecholate	$4^-/3^-$	−1.53	−0.90	−1.37	−0.83
Ti Salicylate[41]	$3^-/2^-$	−0.57	−0.32	−0.52	−0.76
Ti Catecholate[41]	$3^-/2^-$	−1.09	−0.63	−1.34	−1.10
Ti Pyrogallol[41]	$3^-/2^-$	−0.98	−0.57	−1.37	−1.13
Fe $DcBpy_1CN_4$[42]	$4^-/3^-$	0.08	0.06	1.09	0.63
Fe $DcBpy_2CN_2$[42]	$4^-/3^-$	0.35	0.22	0.85	0.88
Fe Bipyridine[43]	$2^+/3^+$	0.90	0.55	0.88	1.12
FePhenanthroline[43]	$2^+/3^+$	−0.19	−0.10	0.98	1.15
Fe $DIPSO_1$[47]	$2^-/1^-$	−1.62	−0.95	−1.08	−0.83
Fe TEA_1[49]	$2^-/1^-$	−1.64	−0.96	−1.27	−0.85
Fe $TIPA_1$[48]	$2^-/1^-$	−1.66	−0.97	−1.27	−0.88
Fe BIS-$TRIS_1$[46]	$4^-/3^-$	−2.84	−1.67	−1.97	−0.91
Fe $Lactate_1$[14]	$0/1^+$	−0.27	−0.15	0.40	0.29
Fe $Lactate_2$[14]	$2^-/1^-$	−0.0027	0.013	−0.20	−0.073
Fe Glycol[14]	$4^-/3^-$	−1.64	−0.96	−0.71	−0.98

Conclusions

In this contribution, we have proposed a DFT protocol for the prediction of reduction potentials of first row transition metal complexes with simple bidentate organic ligands at a modest computational cost and using standard DFT methods. For this, two DFT calculations for each redox form are needed. First, a geometry optimization with a subsequent frequency calculation in the gas phase is performed to obtain the ground state electronic energies and corrections to the free energy. Second, the optimized geometry is used for a COSMO-RS calculation to obtain an estimate of the solvation free energy, or a single point calculation with the SMD solvation model to obtain the total energies in the solvated state.

Among the electronic structure methods evaluated the M06-2X hybrid density functional yielded the closest values to the experimental data set (MAE = 0.56 V vs. 0.77 V using B3LYP). In general, the size and type of basis set used did not have a significant effect on the mean average error. The gaussian type basis set 6311+G(d) resulted in the lowest errors and was consequently chosen for the remaining calculations. The solvation model had the biggest effect on accuracy, with MAE dropping from 0.56 V for using the SMD implicit solvation model to 0.24 using the COSMO-RS model, which combines quantum chemistry with statistical thermodynamics. This, along with the outliers being the complexes with high charges, indicates that the high errors seen with implicit solvation could be due to the loss of specific solvent-solute interactions. In the case where only similar ligands are used, linear regression corrections could be used with the SMD implicit solvation model to significantly reduce errors (MAE = 0.051 V using corrections vs. 0.38 V using M06-2X/6311+G(d)/SMD for the initial set of high spin iron(III) complexes with catechol-like ligands).

Moving forward, the protocol for the determination of the reduction potentials of such complexes could be used to guide experimental work by providing predictions of suitable mediators that could have exact matching to a given insertion material for RT-RFB. Once a complex with a similar enough potential to the solid is identified, this protocol could be used to study the modulations of the redox potential that occur with the addition or substitution of functional groups on the ligand, thus identifying a more suitable complex that would have a perfect match of potential. Furthermore, the DFT protocol could be integrated into a high throughput screening method.

Experimental Section

Computational methods

The standard redox potential U_{red} of the reaction $Fe^{III}L_x + e^- \rightleftharpoons Fe^{II}L_x$ can be calculated from the Gibbs free energy $\Delta G_{red(aq)}$ of the redox reaction, as seen in Equation (1):[20]

$$U_{red} = \frac{-\Delta G_{red(aq)}}{F} - U_{SHE} \quad (1)$$

Where F is Faraday's constant, and U_{SHE} is the potential of the standard hydrogen electrode, considered 4.47 V.[50] $\Delta G_{red(aq)}$ can be calculated from the difference between the calculated electronic energies of the reduced and oxidized forms of the compound in solution ($\Delta E_{(aq)}$), and the difference in thermal corrections to the Gibbs free energies ($\Delta G_{cor(gas)}$) and the zero point energy obtained from frequency calculations in the gas phase using equation 2:

$$\Delta G_{red(aq)} = \Delta E_{(aq)} + \Delta G_{corr(gas)} \quad (2)$$

$\Delta E_{(aq)}$ could be obtained directly, by optimizing geometries in the solvated phase, in which case the calculated electronic energies will be those of the solvated phases and could be used to directly calculate $\Delta E_{(aq)}$. Alternatively, the indirect method could be used, where the energies in the solvated state are obtained from solvated-state single point calculations on geometries optimized in the gas phase.

To obtain the electronic energies of the species in solution $E_{(aq)}$, the most computationally efficient method for considering the effects of the environment is to use implicit solvation models like the polarization continuum model (PCM),[51] the conductor-like screening model (COSMO),[24,52] or the SMD model.[53] In these models, the solute is placed in a cavity located in a polarizable continuum that represents the solvent. The interaction of point charges on the cavity surface with the electronic density of the solute is then used to obtain the total electronic energy $E_{(aq)}$.

We first performed DFT calculations using the B3LYP hybrid density functional, which is a popular choice for ground-state calculations of both organic and transition metal compounds,[32,54] using the Amsterdam Density Functional (ADF)[23] software version 2019.302 and the Gaussian 16[36] software. In ADF, the TZP basis set (triple zeta polarized),[26] numerical frequencies, and COSMO[24] and SM12[25] solvation models for single point calculations were used, while in Gaussian 16 geometry optimizations and analytical frequency calculations were performed using 6-31+G(d),[37] 6-311+

G(d),[38] and cc-pVTZ[39] basis sets and single point calculations performed using the SMD[53] model.

Some of the ligands are not symmetric, with functional groups that do not bond with the metal center, (deferiprone, kojic acid, salicylic acid, pyrogallol) in which case two isomers are possible (Figure S1). For such complexes the geometries of both isomers were optimized, and the average energies were predicted using the Boltzmann distribution and used to calculate the redox potentials.

Some of the ligands have supplementary hydroxyl or carboxyl functional groups that do not bond with the metal center. Their protonation, or lack thereof, was considered depending on their pK_a and pH of complexation or depending on their use in the RFB literature. The hydroxyl groups on kojic acid, pyrogallol, and BIS-TRIS were considered protonated. That of kojic acid has a pK_a of 7.7,[55] while the complex forms at a pH of 4.5. Similarly, the pK_a of the third hydroxyl group in pyrogallol is 14,[56] while the complex is reported to form at a pH of 9.8.[41] The hydroxyl groups of BIS-TRIS are reported to have high pK_a,[57] and are similarly considered protonated by Shin *et al.* in their study on an all iron RFB using iron BIS-TRIS and ferrocyanide.[46] The functional groups of DcBpy were considered deprotonated when complexed. The experimental reduction potential for the iron DcBpy complex is taken from the work of Li *et al.* on aqueous redox flow batteries with neutral-to-alkaline pH,[42] who also considered the carboxyl groups to be deprotonated. The sulfonate group of DIPSO is considered deprotonated as it is expected to have a low pK_a, and the experimental reduction potential of the iron DIPSO complex is from the work of Shin et al. on a highly alkaline aqueous redox flow battery.[47]

Synthesis and characterization

The solutions of iron complexes were prepared by simple mixing of the precursors. Considering the usual coordination number of iron(III), the solutions were prepared in a stoichiometric ratio of metal to bidentate ligand (1:3). The complexes were prepared at a metal concentration of 10 mM, as the maximum concentration was limited by the solubility of the maltol ligand, except for the iron catechol complex which was prepared at 0.5 M concentration due to instability at lower concentrations.

The preparation of the complexes begins by preparing a 0.5 M solution of the supporting salt by dissolving 2.1306 g of sodium sulfate (Acros Organics, 99.5%) into 30 mL of distilled water. Next, the needed mass of ligand solid is dissolved into this solution. Upon complete dissolution of the ligand, 0.1470 g of iron(III) sulfate pentahydrate (Fischer Scientific, general-purpose grade) is added. The solution is stirred at room temperature for one hour before the pH is adjusted *via* dropwise addition of sodium hydroxide solution (Sigma Aldrich, 98%, pellets). If too much base was added, the pH is regulated using diluted sulfuric acid solution (Fischer Scientific, 95% w/w solution). The solutions are stirred for another hour before electrochemical characterization. The ligands used were kojic acid (Alfa Aesar, 99%), maltol (Alfa Aesar, 99%), deferiprone (Acros Organics, 99+%), and catechol (Alfa Aesar, 99%). All reagents were used without further purification.

Electrochemical characterization of the complexes was performed using a three-electrode setup and a VSP potentiostat from Biologic. A standard saturated calomel electrode from Radiometer Analytical, filled with a potassium chloride solution and protected from the analyte using a standard R-AL120 bridge tube from Biologic filled with supporting electrolyte solution was used as a reference. The potentials are recalculated to be reported as vs. the standard hydrogen electrode (SHE). The counter electrode consisting of carbon paper, and the working electrode was made of glassy carbon (2 mm Ø). Prior to each measurement, the working electrode was pretreated using a method adapted from that of Savant et al.[58] First, the electrode was polished using aluminum oxide powder (grain size 0.3 μm) before being rinsed and sonicated for 30 s. It was then rerinsed and activated by cycling in 0.5 M sulfuric acid solution for 80 cycles in the potential range of −0.05 V to +1.71 V vs. SHE at a scan rate of 200 mV s^{-1}. The electrode was then rinsed one last time and immersed in the analyte solution, purged for 15 min using 99.9% Argon before performing cyclic voltammetry (CV) scans with a 200 mV s^{-1} scan rate (Figure S2). All reported potentials are with respect to the standard hydrogen electrode (SHE). To verify the formation of the ML3 complexes, the evolution of the complexes with pH was tracked using a Carry Series UV/Vis/NIR spectrophotometer from Agilent Technologies; the experimental redox potentials used for the DFT study correspond to the ML3 complexes at their required pH (Figure 1, S3).

Acknowledgements

The authors acknowledge the ALISTORE European Research Institute for funding support.

Conflict of Interests

The authors declare no conflict of interest.

Data Availability Statement

The data that support the findings of this study are available in the supplementary material of this article.

Keywords: redox potential · transition metal complex · density functional theory · redox flow batteries · redox targeting

[1] H. Zhang, C. Sun, *J. Power Sources* **2021**, *493*, 229445.
[2] T. N. Pham-Truong, Q. Wang, J. Ghilane, H. Randriamahazaka, *ChemSusChem* **2020**, *13*, 2142–2159.
[3] Q. Huang, H. Li, M. Grätzel, Q. Wang, *Phys. Chem. Chem. Phys.* **2013**, *15*, 1793–1797.
[4] G. Lee, C. M. Wong, C. S. Sevov, *ACS Energy Lett.* **2022**, *7*, 3337–3344.
[5] M. Zhou, Q. Huang, T. N. Pham Truong, J. Ghilane, Y. G. Zhu, C. Jia, R. Yan, L. Fan, H. Randriamahazaka, Q. Wang, *Chem* **2017**, *3*, 1036–1049.
[6] H. Zhang, Q. Huang, X. Xia, Y. Shi, Y.-M. Shen, J. Xu, Z. Chen, J. Cao, *J. Mater. Chem. A* **2022**, *10*, 6740–6747.
[7] E. Schröter, C. Stolze, A. Saal, K. Schreyer, M. D. Hager, U. S. Schubert, *ACS Appl. Mater. Interfaces* **2022**, *14*, 6638–6648.
[8] M. Zhou, Y. Chen, M. Salla, H. Zhang, X. Wang, S. R. Mothe, Q. Wang, *Angew. Chem. Int. Ed.* **2020**, *59*, 14286–14291.
[9] T. Páez, F. F. Zhang, M. Á. Muñoz, L. Lubian, S. Xi, R. Sanz, Q. Wang, J. Palma, E. Ventosa, *Adv. Energy Mater.* **2022**, *12*, 2102866.
[10] E. Zanzola, S. Gentil, G. Gschwend, D. Reynard, E. Smirnov, C. R. Dennison, H. H. Girault, P. Peljo, *Electrochim. Acta* **2019**, *321*, 134704.
[11] Y. Cheng, X. Wang, S. Huang, W. Samarakoon, S. Xi, Y. Ji, H. Zhang, F. Zhang, Y. Du, Z. Feng, S. Adams, Q. Wang, *ACS Energy Lett.* **2019**, *4*, 3028–3035.
[12] M. Moghaddam, S. Sepp, C. Wiberg, A. Bertei, A. Rucci, P. Peljo, *Molecules* **2021**, *26*, 2111.
[13] M. A. Rizvi, M. Mane, M. A. Khuroo, G. M. Peerzada, *Monatsh. Chem.* **2017**, *148*, 655–668.

[14] A. J. Esswein, J. Goelts, E. R. King, S. Y. Reece, D. Almadeo, in *Aqueous Redox Flow Batteries Comprising Metal Ligand Coordination Compounds*, **2013**, US8753761B2.
[15] J. Gao, K. Amini, T. Y. George, Y. Jing, T. Tsukamoto, D. Xi, R. G. Gordon, M. J. Aziz, *Adv. Energy Mater.* **2022**, *12*, 2202444.
[16] P. de Silva, in *Flow Batteries* (Eds.: C. Roth, J. Noack, M. Skyllas-Kazacos), Wiley, **2023**, pp. 333–354.
[17] S. Er, C. Suh, M. P. Marshak, A. Aspuru-Guzik, *Chem. Sci.* **2015**, *6*, 885.
[18] Y. Moon, Y. K. Han, *Curr. Appl. Phys.* **2016**, *16*, 939–943.
[19] Q. Zhang, A. Khetan, E. Sorkun, F. Niu, A. Loss, I. Pucher, S. Er, *Energy Storage Mater.* **2022**, *47*, 167–177.
[20] R. P. Fornari, P. de Silva, *Wiley Interdiscip. Rev.: Comput. Mol. Sci.* **2021**, *11*, e1495.
[21] A. Nandy, C. Duan, M. G. Taylor, F. Liu, A. H. Steeves, H. J. Kulik, *Chem. Rev.* **2021**, *121*, 9927–10000.
[22] J. P. Janet, S. Ramesh, C. Duan, H. J. Kulik, *ACS Cent. Sci.* **2020**, *6*, 513–524.
[23] G. Te Velde, F. M. Bickelhaupt, E. J. Baerends, C. Fonseca Guerra, S. J. A. Van Gisbergen, J. G. Snijders, T. Ziegler, *J. Comput. Chem.* **2001**, *22*, 931-967.
[24] C. C. Pye, T. Ziegler, *Theor. Chem. Acc.* **1999**, *101*, 396–408.
[25] C. A. Peeples, G. Schreckenbach, *J. Chem. Theory Comput.* **2016**, *12*, 4033–4041.
[26] E. Van Lenthe, E. J. Baerends, *J. Comput. Chem.* **2003**, *24*, 1142–1156.
[27] A. Klamt, *Wiley Interdiscip. Rev.: Comput. Mol. Sci.* **2018**, *8*, e1338.
[28] C. C. Pye, T. Ziegler, E. Van Lenthe, J. N. Louwen, *Can. J. Chem.* **2009**, *87*, 790–797.
[29] P. Verma, Z. Varga, J. E. M. N. Klein, C. J. Cramer, L. Que, D. G. Truhlar, *Phys. Chem. Chem. Phys.* **2017**, *19*, 13049–13069.
[30] SCM, "ADF User Manual – ADF COSMO calculation settings," can be found under http://www.scm.com/doc/COSMO-RS/ADF_COSMO_calculation.html#adf-cosmo-settings.
[31] E. Van Lenthe, *J. Chem. Phys.* **1999**, *110*, 8943–8953.
[32] L. P. Wang, T. Van Voorhis, *J. Chem. Theory Comput.* **2012**, *8*, 610–617.
[33] R. P. Fornari, P. de Silva, *Molecules* **2021**, *26*, 3978.
[34] T. Weymuth, E. P. A. Couzijn, P. Chen, M. Reiher, *J. Chem. Theory Comput.* **2014**, *10*, 3092–3103.
[35] R. V. Listyarini, D. S. Gesto, P. Paiva, M. J. Ramos, P. A. Fernandes, *Front. Chem.* **2019**, *7*, 391.
[36] M. J. Frisch, G. W. Trucks, H. B. Schlegel, G. E. Scuseria, M. A. Robb, J. R. Cheeseman, G. Scalmani, V. Barone, G. A. Petersson, H. Nakatsuji, X. Li, M. Caricato, A. V. Marenich, J. Bloino, B. G. Janesko, R. Gomperts, B. Mennucci, H. P. Hratchian, J. V. Ortiz, A. F. Izmaylov, J. L. Sonnenberg, D. Williams-Young, F. Ding, F. Lipparini, F. Egidi, J. Goings, B. Peng, A. Petrone, T. Henderson, D. Ranasinghe, V. G. Zakrzewski, J. Gao, N. Rega, G. Zheng, W. Liang, M. Hada, M. Ehara, K. Toyota, R. Fukuda, J. Hasegawa, M. Ishida, T. Nakajima, Y. Honda, O. Kitao, H. Nakai, T. Vreven, K. Throssell, J. A. Montgomery, J. E. Peralta, F. Ogliaro, M. J. Bearpark, J. J. Heyd, E. N. Brothers, K. N. Kudin, V. N. Staroverov, T. A. Keith, R. Kobayashi, J. Normand, K. Raghavachari, A. P. Rendell, J. C. Burant, S. S. Iyengar, J. Tomasi, M. Cossi, J. M. Millam, M. Klene, C. Adamo, R. Cammi, J. W. Ochterski, R. L. Martin, K. Morokuma, O. Farkas, J. B. Foresman, D. J. Fox, **2016**.
[37] G. A. Petersson, M. A. Al-Laham, *J. Chem. Phys.* **1991**, *94*, 6081–6090.
[38] K. Raghavachari, G. W. Trucks, *J. Chem. Phys.* **1989**, *91*, 1062–1065.
[39] R. A. Kendall, T. H. Dunning, R. J. Harrison, *J. Chem. Phys.* **1992**, *96*, 6796–6806.
[40] S. J. Konezny, M. D. Doherty, O. R. Luca, R. H. Crabtree, G. L. Soloveichik, V. S. Batista, *J. Phys. Chem. C* **2012**, *116*, 6349–6356.
[41] A. J. Esswein, S. Y. Reece, J. Goeltz, E. R. King, D. Amadeo, N. Tyagi, T. D. Jarvi, in *Electrochemical Energy Storage Systems and Methods Featuring Large Negative Half-Cell Potentials*, **2017**, US 9,559,374 B2.
[42] X. Li, P. Gao, Y. Y. Lai, J. D. Bazak, A. Hollas, H. Y. Lin, V. Murugesan, S. Zhang, C. F. Cheng, W. Y. Tung, Y. T. Lai, R. Feng, J. Wang, C. L. Wang, W. Wang, Y. Zhu, *Nat. Energy.* **2021**, *6*, 873–881.
[43] J. G. Ibanez, C. Choi, R. S. Becker, *J. Electrochem. Soc.* **1987**, *134*, 3083.
[44] G. Liang, N. J. DeYonker, X. Zhao, C. E. Webster, *J. Comput. Chem.* **2017**, *38*, 2430–2438.
[45] T. F. Hughes, R. A. Friesner, *J. Chem. Theory Comput.* **2012**, *8*, 442–459.
[46] M. Shin, S. Oh, H. Jeong, C. Noh, Y. Chung, J. W. Han, Y. Kwon, *Int. J. Energy Res.* **2022**, *46*, 8175–8185.
[47] M. Shin, C. Noh, Y. Chung, Y. Kwon, *Chem. Eng. J.* **2020**, *398*, 125631.
[48] C. Noh, Y. Chung, Y. Kwon, *Chem. Eng. J.* **2021**, *405*, 126966.
[49] C. Noh, Y. Chung, Y. Kwon, *J. Power Sources* **2020**, *466*, 228333.
[50] O. Hammerich, B. Speiser, *Organic Electrochemistry, Fifth Edition: Revised and Expanded*, **2015**.
[51] S. Miertus, E. Scrocco, J. Tomasi, *Chem. Phys.* **1981**, *55*, 117–129.
[52] A. Klamt, *J. Phys. Chem.* **1995**, *99*, 2224–2235.
[53] A. v. Marenich, C. J. Cramer, D. G. Truhlar, *J. Phys. Chem. B* **2009**, *113*, 6378–6396.
[54] T. Matsui, Y. Kitagawa, Y. Shigeta, M. Okumura, *J. Chem. Theory Comput.* **2013**, *9*, 2974–2980.
[55] V. M. Nurchi, G. Crisponi, J. I. Lachowicz, S. Murgia, T. Pivetta, M. Remelli, A. Rescigno, J. Niclós-Gutíerrez, J. M. González-Pérez, A. Domínguez-Martín, A. Castiñeiras, Z. Szewczuk, *J. Inorg. Biochem.* **2010**, *104*, 560–569.
[56] R. M. Smith, A. E. Martell, in *Critical Stability Constants*, Volume 2, 212, Plenum Press, New York and London, **1990**.
[57] K. Scheller, T. Abel, P. Polanyi, P. Wenk, B. Fischer, H. Sigel, *Eur. J. Biochem.* **1980**, *107*, 455–466.
[58] T. v. Sawant, J. R. McKone, *J. Phys. Chem. C* **2018**, *123*, 144–152.

Manuscript received: April 4, 2023
Revised manuscript received: May 23, 2023
Accepted manuscript online: May 25, 2023
Version of record online: July 18, 2023